Characterizing the parallax error in multi-pinhole micro-SPECT reconstruction

B. Vandeghinste, *Student Member, IEEE,* J. De Beenhouwer, R. Van Holen, *Member, IEEE,* S. Vandenberghe, and S. Staelens

***Abstract*—The usage of pinholes is very important in preclinical micro-SPECT. Pinholes can magnify the object onto the detector, resulting in better system resolutions than the detector resolution. The loss in sensitivity is usually countered by adding more pinholes, each projecting onto a specific part of the detector. As a result, gamma rays have an oblique incidence to the detector. This causes displacement and increased uncertainty in the position of the interaction of the gamma ray in the detector, also known as parallax errors or depth-of-interaction (DOI) errors. This in turn has a large influence on image reconstruction algorithms using ray tracers as a forward projector model, as the end-point of each ray on the detector has to be accurately known.**

In this work, we used GATE to simulate the FLEX Triumph-I system (Gamma Medica-Ideas, Northridge, CA), a CZT-based multi-pinhole micro-SPECT system. This system uses 5 mm thick CZT pixels, with 1.5 mm pixel pitch. The simulated information was then used to enhance the image resolution by accurately modeling the DOI. Two hundred point sources were simulated and rebinned to use the DOI information. This data was then used in a GPU-based iterative reconstruction algorithm taking the simulated DOI into account. The average displacement was then determined for all point sources, and the FWHM was calculated in three dimensions, by fitting the point sources with 3D Gaussians. We show that the displacement is reduced by 83% on average. We also show a 15% resolution gain when only 5 DOI levels are used.

I. Introduction

THE usage of pinholes is very important in preclinical micro-SPECT. Pinholes can magnify the object onto the detector, resulting in a better system resolution than detector resolution. The loss in sensitivity is usually countered by using multiple pinholes per collimator, each pinhole projecting onto one specific part of the detector. Such imaging geometry implies oblique incidence of gamma rays to the detector. This causes displacement and increased uncertainty in the position of the interaction of the gamma ray in the detector. These errors are known as parallax errors or depth-of-interaction (DOI) errors.

The DOI effect can accurately be compensated for when the systematic imperfections are compensated by measuring the system response at a grid of discrete locations in the field of view (FOV) of the camera. Unfortunately, this reponse can not always be reliably measured on different systems, due to difficulty to position a point source in such a grid of locations. Moreover, these measurements are especially tedious for non-stationary systems. A different approach to compensate for the DOI effect is to directly incorporate the physical processes leading to the effect into the reconstruction. A more accurate forward projection operator will then provide projections closer to the measured data.

In a ray-driven forward projector, each ray is connected from the middle of one certain detector pixel to a pinhole, and then traced through the voxel space (Fig. 1). A simplified model would put the detector end-points at the depth corresponding with the mean free path for this specific isotope and this specific detector material. For ^{99m}Tc, this is at approximately 2.57 mm depth in CZT detectors. The DOI essentially determines the angle of each traced ray. A wrong estimation of the DOI could thus lead to wrong sampling of the voxel space. This effect will be most apparent at the edge of the FOV for each individual pinhole. Furthermore, this effect will be larger for relatively thick detector materials compared to the detector pixel width, which is the case for CZT detectors. These detectors have high energy resolution, high intrinsic spatial resolution, good detection efficiency and a high count rate [1], making them a good choice for preclinical SPECT imaging. The DOI effect has previously been reported for CsI and HPGe detectors [3].

The aim of this work is to characterize the influence of the parallax error and investigate the possible gains of modeling this physical effect in reconstruction directly, specifically for a multi-pinhole micro-SPECT system with pixellated CZT detectors. It has been shown that depth information can be obtained by determining the correlation between a signal's amplitude and its rise time [2], although this is no standard practice yet. It could thus be beneficial to compensate for this effect without measuring the DOI directly, e.g. through system simulations.

II. Materials and Methods

A. SPECT camera model

The FLEX Triumph-I system (Gamma-Medica Ideas, Northridge, CA, USA) was used as a model for a typical multi-pinhole CZT-based micro-SPECT scanner. This preclinical

Manuscript received November 10, 2011. This work was supported in part by a PhD grant to Bert Vandeghinste of the Institute for the Promotion of Innovation through Science and Technology in Flanders (IWT-Vlaanderen), a postdoctoral fellowship of the Research Foundation Flanders (FWO) to Roel Van Holen, and by the CIMI project, an IBBT-project in cooperation with: Barco nv, DCILABS, IBA Dosimetry, GE and DSC Labs. IBBT is an independent multidisciplinary research institute founded by the Flemish Government, to stimulate ICT innovation.

Bert Vandeghinste, Jan De Beenhouwer, Roel Van Holen, Stefaan Vandenberghe and Steven Staelens are with the Department of Electronics and Information Systems, MEDISIP, Ghent University–IBBT–IBiTech, De Pintelaan 185 block B, B-9000 Ghent, Belgium (e-mail: bert.vandeghinste@ugent.be).

J. De Beenhouwer is also with The Vision Lab, University of Antwerp, 2610 Wilrijk, Belgium.

S. Staelens is also with the Molecular Imaging Centre Antwerp, University of Antwerp, 2650 Edegem, Belgium.

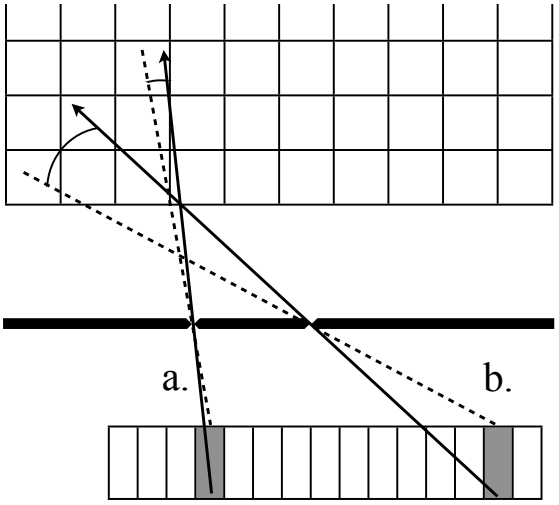

Fig. 1: Ray tracing in pixel-driven projectors. Grey pixels show the detected events. The difference between the solid and dotted lines shows the possible angles for the projection operators. (a) Little influence for relatively straight rays. (b) A larger oblique angle leads to a larger parallax error. Only the detector pixel width (1.5 mm) and height (5 mm) are to scale.

tri-modal PET/SPECT/CT system consists of four 80-by-80 pixels CZT detector heads with 1.6 mm pixel width and 5 mm pixel depth. Each head is fitted with a 5-pinhole Tungsten collimator. The pinhole diameters are specified at 0.5 mm and the opening angle is 32 degrees. The focal length is 75 mm and the rotation axis-detector distance was 42 mm, giving a magnification factor of 1.79.

The methods developed by Bequé et al. [4], [5] were used to accurately calibrate the SPECT geometry. The measured projections from three ^{99m}Tc point sources embedded in an acrylic disk phantom were segmented and analyzed to find the 15 centroids per projection angle per detector head. All centroids were then used in an optimization scheme, resulting in the focal length and the location for each pinhole, the distance between the detector and the rotation axis, the offset of the detector center, the detector tilt and skew and the angle offset between the 4 detector heads.

B. Monte Carlo Simulation

An accurate representation of this system was built in the GEANT4-based GATE v3.1.2 [6], which had been improved with forced-detection to speed up the simulation process [7]. The CZT cameras were modeled (Fig. 2) to ensure realistic attenuation and scattering in the detector itself by using the correct material properties and thicknesses.

The data was generated by placing two hundred ^{99m}Tc point sources (6.5 MBq each) 10 mm apart spherically from each other in one volume. The number of projection views was set to 60 views over 360 degrees. All data was stored as ROOT[1] output, which allows us to post-process all acquired

[1]A Data Analysis Framework, http://root.cern.ch

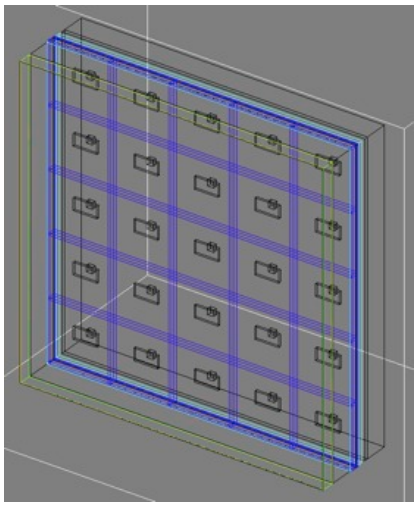

Fig. 2: CZT detector modeled in GATE.

data without having to re-simulate the photon incidence on the detector.

C. Processing

Two different sets of data were generated from the ROOT output. The first dataset was rebinned to simulate a detector with no DOI information, by summing all detected events according to the location of their respective deposited energy. This can be regarded as the function of CZT in the current available systems.

The second dataset is generated out of the same data, but binned into 5 DOI levels, by uniformly quantizing the depth of each deposited ray. A histogram of the depth was stored simultaneously per pixel (Fig. 3). Fig. 4 shows the histogram for events inside the photopeak. This removes the scattering events inside the detector.

A second simulation generated a third dataset, where a highly attenuating material replaced the CZT detector. This setup simulates a perfect absorber. All events were absorbed instantly when the detector was hit. This data serves as a reference to the other datasets, as no parallax error can occur. This allows us to investigate the best possible results in the ideal case.

D. Reconstruction

A reconstruction algorithm was developed for multi-pinhole micro-SPECT imaging. This algorithm consists of a ray-driven forward projector and a voxel-driven back projection. These are combined in the iterative OSEM algorithm. Pinhole resolution recovery was based on a multi-ray approach using 7 rays [8]. These 7 rays intersect the circular opening of the pinhole in a hexagonal pattern with one of the points in the centre. This effectively subsamples the pinhole.

Pinhole penetration was taken into account by calculating the effective pinhole diameter d_r using the nominal diameter d, the acceptance angle of the pinhole α and the attenuation of the collimator material μ as parameters [9]:

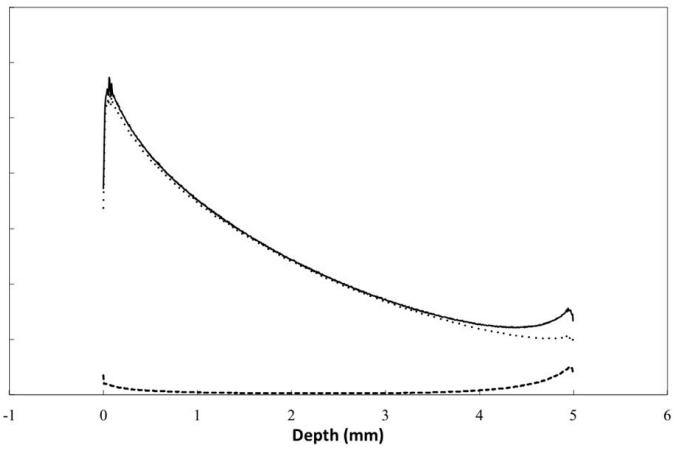

Fig. 3: Histogram of detected photons according to depth of detection. Full line: measured DOI. Dashed line: scattered photons. Dotted line: photonscatter free.

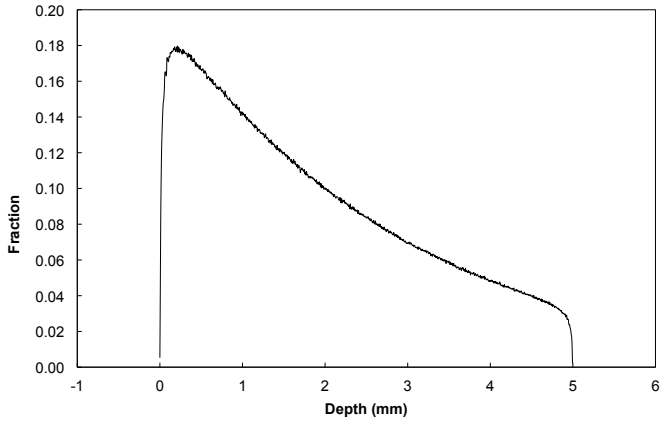

Fig. 4: Histogram of photon detection depth, for photons in the photopeak window.

$$d_r = \sqrt{d\left(d + \frac{2}{\mu}\tan\frac{\alpha}{2}\right)}. \tag{1}$$

Three different volumes were reconstructed:

1) For the non-ideal single-layer dataset, 7 rays were traced from the center of each detector pixel – at a depth equal to the mean free path – trough the pinhole, calculating which voxels to sample along the ray.
2) For the 5-layer dataset, 7 rays were drawn per pixel per DOI layer. The endpoint of each ray was chosen to be in the centre of each layer. The sampled voxel values along this ray were then multiplied by the fraction of photons received by each layer, as determined by the simulations (Fig. 4). This amounts to weighted subsampling of the DOI per pixel. For the back projector, the same principle was applied, but without taking the photon fraction into account.
3) The reference dataset was reconstructed similarly to the single-layer dataset, putting the end point of each ray at the top plate of the detector.

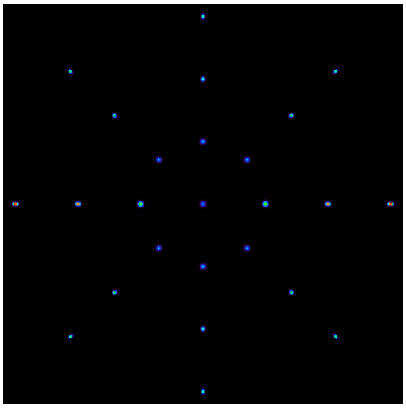

Fig. 5: Central slice of data reconstructed with 5 DOI levels.

All datasets were reconstructed to a $320 \times 320 \times 320$ voxel space with a $0.2 \times 0.2 \times 0.2$ mm^3 voxel pitch. All voxel samples were determined through 3D texture interpolation in CUDA. This leads to blobs with only a small discretization error. The data was reconstructed using 5 iterations and 6 subsets. These parameters lead to a 2-minute reconstruction time when DOI is not corrected for, and 10 minutes reconstruction time when 5 DOI levels are used. All reconstruction software was implemented in CUDA, and ran on a Tesla M2070 GPU (NVIDIA, Santa Clara, CA, USA).

E. Post-processing

The reconstructed images were automatically segmented and scanned for all point sources. Three 2D Gaussians were fitted to each point source inside a $20 \times 20 \times 20$ pixels window, resulting in a mean location of the peak $\mu_{x,y,z}$ and a standard deviation $\sigma_{x,y,z}$. The x-axis is defined as being perpendicular to the detector face, the y-axis as the tangential, and the z-axis as parallel to the rotational axis.

As a first measure, the location was compared to the positions of the point sources from the ideal simulation, using the ℓ_2-norm of the difference between those locations (in mm):

$$\text{cost} = \frac{1}{n}\sum_n ||\vec{p}_n - \vec{\mu}_n||_2^2, \tag{2}$$

with $\vec{\mu}$ the estimated peak position, $\vec{p}$ the reference position from the simulation with the perfect absorber (Section II-C) and n the number of point sources measured. This metric thus represents the displacement caused by inaccurate DOI modeling.

As a second measure, the full-width-at-half-maximum (FWHM) was compared to the FWHM of the ideal simulation results, to quantify the loss in resolution when DOI is not adequately accounted for:

$$\text{FWHM}_{x,y,z} = 2\sqrt{2\ln 2}\sigma_{x,y,z}. \tag{3}$$

III. Results

Figure 5 shows data reconstructed with 5 DOI levels, showing how the outside FWHMs have broadened compared

TABLE I: Averaged results (mean±std.dev., in mm).

	FWHM$_x$	FWHM$_y$	FWHM$_z$	Displacement
Perfect Absorber	0.483±0.110	0.422±0.162	0.463±0.111	0.000
No DOI	0.568±0.054	0.469±0.150	0.557±0.204	0.333
5 DOI levels	0.471±0.049	0.406±0.121	0.486±0.143	0.057
Increase	**17.08%**	**14.33%**	**12.75%**	-

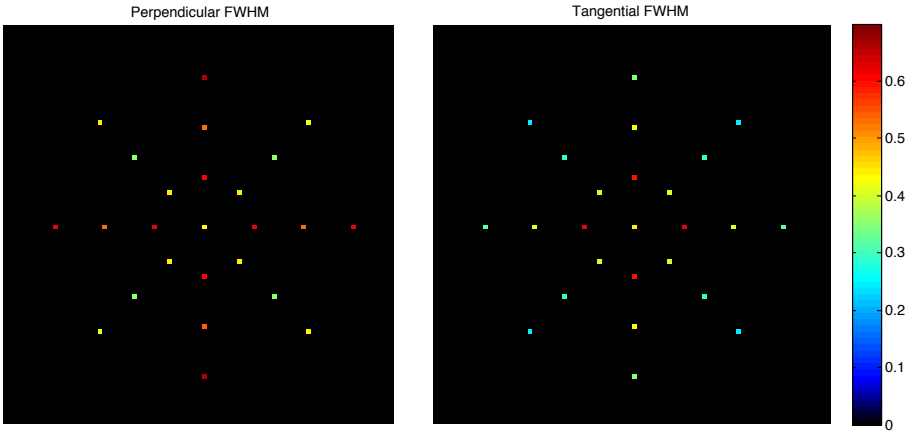

(a) (b)

Fig. 6: Two color coded plots showing (a) the perpendicular FWHM and (b) the tangential FWHM.

to the central FWHM. Figure 6 shows the mean location of the point sources reconstructed from 5 DOI levels. The point sources have been color coded to show FWHM$_x$ and FWHM$_y$. All figures show the central slice.

The displacement cost for all point sources combined was found to be at 0.333 mm when no DOI information was available. This improved to 0.057 mm total displacement when 5 depth levels were modeled.

The perpendicular resolution gain with 5-level DOI modeling is 0.117 mm in the center to 0.054 mm on the outside, or a 19.4% to 10.4% increase in resolution. The tangential FWHM shows a 0.072 mm (12.7%) increase in resolution in the center, and a 0.030 mm (10%) increase in resolution on the outside. The axial FWHM increases by 0.007 to 0.099 mm (2.1% to 15.0%). These results have been averaged and are summarized in Table I.

IV. Discussion

The photoelectric effect is the main contributor to the DOI histogram shown on Fig. 3. Simulations show that scattered photons have a large presence near the top and the bottom of the detector. The photons at the bottom are primarily caused by backscatter, depositing low energy photons directly after changing direction. This leads to a larger influence for the deepest possible rays. Both scatter fractions can be minimized by windowing the photopeak energy. The resulting DOI information is shown on Fig. 4. This can be solved for other isotopes by building an accurate attenuation model for the detector and quantifying the photon fractions as shown in Section II-A.

The results clearly show that the parallax effect is the cause of two main problems. A first problem is the broadening of the FWHMs, leading to resolution loss in the reconstructed images. A significantly higher resolution is possible both perpendicularly as well as tangentially. The influence increases when moving radially outward, and can thus be regarded as a 3D magnification effect.

A second problem is the displacement of point sources. This displacement is of major importance in SPECT/CT systems. Usually, co-registration is very simple on these systems as the SPECT and CT are located on the same gantry. With this displacement, only the central region would be perfectly co-registered, and a large mismatch would be noted for voxels on the outside of the FOV. As the CT image is used to correct for attenuation and the partial volume effect, it is very important that there is no mismatch. It was shown that this effect could be corrected for by using good DOI modeling. Although conventional detectors lead to an on average 0.333 mm displacement of the pointsources, this converges to almost 0 when 5 DOI levels are used.

V. Conclusion

We have characterized the parallax error for a CZT-based multi-pinhole micro-SPECT system. The DOI should be corrected for when SPECT is using CT as a correction map, as a mismatch between SPECT and CT voxels is unavoidable otherwise. Each point source was displaced 0.333 mm on average when no DOI modeling was added. This displacement was reduced to 0.057 mm with the introduction of 5 DOI levels. The axial resolution increased with 15%, while the transaxial resolution increased with an average of 71 μm, which is in the range of 13%. This characterization shows the importance of modeling the DOI in multi-pinhole micro-

SPECT systems, when using relatively thick detectors such as 5-mm CZT.

In the future, we will investigate the possibilities of on-the-fly correction of this effect during ray tracing. The information from this study will be used to model this effect accurately in reconstruction itself, without prior knowledge of the DOI.

ACKNOWLEDGMENT

The authors would like to thank Dirk Meier of Gamma-Medica Ideas for his help and comments on CZT detector modeling.

REFERENCES

[1] T. Funk et al., *A new CdZnTe-based gamma camera for high resolution pinhole SPECT*, IEEE NSS Conference Record, 2004.

[2] L. Guerin, L. Verger, V. Rebuffel and O. Monnet, *A New Architecture for Pixellated Solid State Gamma Camera Used in Nuclear Medicine*, IEEE Trans Nuc Sci, vol. 55, no. 3, pp. 15731580, 2008.

[3] A. B. Hwang, K. Iwata and B. H. Hasegawa, *Simulation of depth of interaction effects for pinhole SPECT*, IEEE NSS Conference Record, 2001.

[4] D. Bequé, J. Nuyts, G. Bormans, P. Suetens and P. Dupont, *Characterization of acquisition geometry of pinhole SPECT*. IEEE Trans Med Imag, vol. 22, no. 5, pp. 599-612, 2003.

[5] D. Bequé, J. Nuyts, P. Suetens and G. Bormans, *Optimization of geometrical calibration in pinhole SPECT*, IEEE Trans Med Imag, vol. 24, no. 2, pp. 180-190, 2005.

[6] S. Jan et al. *GATE: a simulation toolkit for PET and SPECT*, Phys Med Biol, vol. 49, pp. 4543-4561, 2004.

[7] J. De Beenhouwer, *Fast GATE multi-pinhole SPECT simulations*, Proc of the 2010 MIC, Knoxville, Tennessee, 2010.

[8] C. Vanhove, A. Andreyev, M. Defrise, J. Nuyts and A. Bossuyt, *Resolution recovery in pinhole SPECT based on multi-ray projections: a phantom study*, Eur J Nucl Med Mol Imaging, vol. 34, no. 2, pp. 170-180, 2007.

[9] H. O. Anger, *Radioisotope cameras*, Instrumentation in Nuclear Medicine, G. J. Hine, Ed. New York: Academic, vol. 1, pp. 485-552, 1967.